Journal of Oceanography, Vol. 53, pp. 421 to 433. 1997

Oceanographic Conditions near the Spawning Ground of Southern Bluefin Tuna; Northeastern Indian Ocean

HIROSHI MATSUURA[1]*, TAKASHIGE SUGIMOTO[1], MUNENORI NAKAI[1] and SACHIKO TSUJI[2]

[1]*Ocean Research Institute, University of Tokyo, 1-15-1, Minamidai, Nakano, Tokyo 164, Japan*
[2]*National Research Institute of Far Seas Fisheries, Orido, Shimizu, Shizuoka, Japan*

(Received 16 October 1996; in revised form 21 March 1997; accepted 18 April 1997)

Hydrographic surveys and surface current observations using satellite tracked buoys were conducted from December, 1992 to February, 1993, near the spawning ground of southern bluefin tuna, *Thunnus maccoyii*, in the water between Australia and Indonesia to study the larval feeding and transport environment. The surface of the observation area was covered by warm tropical water. Warm water was also observed along the west coast of Australia extending from the North West Cape. The thickness of the surface mixed layer was about 20 to 50 m and chlorophyll-a concentration in the surface mixed layer was very low. The subsurface chlorophyll maximum lay at 50–75 m. Surface geopotential anomalies along the meridional observation line west of Australia showed an eastward geostrophic flow. The trajectories of satellite tracked drifting buoys revealed a meso-scale dominating current with eddies of about 100–300 km in diameter with a weak mean westward current of about 6 cm/s. Horizontal dispersion coefficients estimated from the Lagrangian auto-correlation function increased almost linearly at first and became almost constant at about 3.6×10^3 m^2/s after about 6 days from release. The influx rate of larvae of southern bluefin tuna into the Leeuwin current was evaluated with a simple diffusion/advection model based on the results of this observation.

Keywords:
· Southern bluefin tuna,
· Northeastern Indian Ocean,
· drifting buoys,
· CTD observations,
· chlorophyll,
· dispersion model,
· Lagrangian statistics,
· eddy.

1. Introduction

Southern bluefin tuna is a highly prized delicacy in Japan. As a resource, it is managed by multi-national agreement between Australia, Japan and New Zealand. However, this species is also caught by some other countries. It is very important to understand the fluctuation of the resource in order to manage it better. Variations of a fish stock can be caused by fishing activities and by variations of environmental and biological factors affecting the recruitment of the stock. Although the spawning ground of southern bluefin tuna is considered to be in a very limited area between Australia and Indonesia (Shinguu, 1981; Nishikawa *et al*., 1985), their juveniles are found off the west coast of Australia. A plausible explanation for this transport from the spawning ground to the nursery ground is not yet available.

Figure 1 shows the region of interest, and the spawning ground of southern bluefin tuna based on the catches of the larvae between 1956 and 1981 (Nishikawa *et al*., 1985) is shown as an area enclosed by a hatched line. The continental shelf of northwestern Australia is very wide (over 200 km), but it becomes very narrow (about 5 km) near North West Cape, the north western corner of Australia. To the south of the North West Cape it is about 50–100 km wide. Major surface currents in this region are Indonesian throughflow (ITF), South Java current (SJC), South Equatorial current (SEC), Eastern Gyral current (EGC) and Leeuwin current (LC), as shown in Fig. 1 (Meyers, 1996). ITF is a current from the Pacific Ocean to the Indian Ocean through the Indonesian seas (Lukas *et al*., 1996; Godfrey, 1996). This flow provides warm but low salinity tropical surface water, which is the result of modifications in Indonesian Seas, to the Indian Ocean (Hautala *et al*., 1996). The estimated transport of this current varies over an order of magnitude (Godfrey, 1996) and recent studies indicate that there are significant seasonal and inter-annual variations, the latter of which is related to the Southern Oscillation Index (SOI) (Meyers, 1996; Fieux *et al*., 1996). The Leeuwin current is a southward flow along the west coast of Australia which is driven by the gradient of steric sea level (Cresswell and Golding, 1980; Godfrey and Ridgway, 1985; McCreary *et al*., 1986; Godfrey and Weaver, 1991). Direct measurements of this current by current meters were made by CSIRO, Australia (Boland *et al*., 1988; Smith *et al*., 1991: The northern most mooring of their extensive project is shown as

*Current affiliation: Japan Marine Science and Technology Center, 2-15, Natsushima-cho, Yokosuka, Kanagawa 237, Japan.

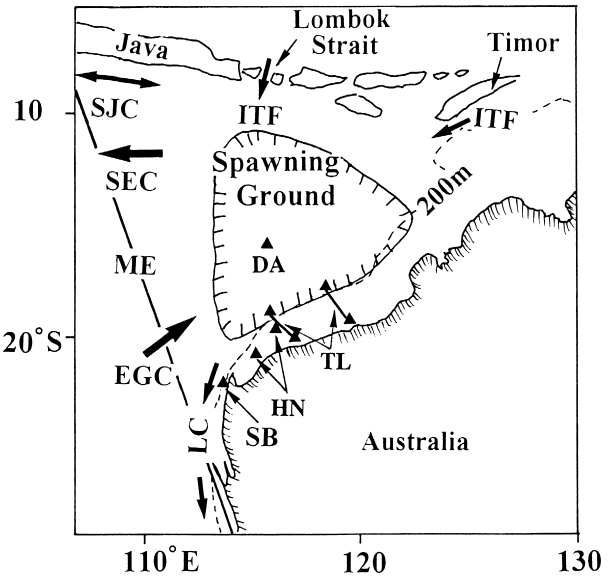

Fig. 1. A map of the region of the spawning ground of Southern bluefin tuna. Thick arrows indicate major surface currents. Solid triangles and lines indicate positions of observations of past research.

SB in Fig. 1). LC may be important for the maintenance of the stock of southern bluefin tune because it may connect the spawning ground to the nursery ground of southern bluefin tuna. Inter-annual variation of currents across the line ME in Fig. 1 has been studied by Meyers (1996) who used XBT records between 1983 and 1994. He showed that the most dominant variation, which is correlated to the SOI, has a maximum amplitude near the Australian coast, the amplitude decreasing northward.

Mean currents near the Australian coast but off the shelf are believed to be northward along the west coast and northeastward north of the North West Cape in the austral summer (Wyrtki, 1961; Tchernia, 1980). High salinity water flows eastward along 30°S and it becomes a southward coastal flow off the west coast of Australia in the austral summer (Hamon, 1965; Andrews, 1977). Holloway and Nye (1985) showed the results of current meter measurements on Australian North West Shelf (HN in Fig. 1) over one year. Their results showed that the monthly average current on the North West Shelf could be southwestward even in February, which was not the season when the Leeuwin current became strong. Cresswell *et al.* (1993) found a surface current, which was observed by satellite tracked buoys west of 120°E, which was northwestward during the northwest monsoon season. However, they also showed that the current observed by current meters near the surface on the shelf was southwestward in this season and they mentioned that the changes of current were 3–4 months ahead of the changes of the wind.

Besides these physical oceanographic studies, the distribution of various properties in this region has also been studied by several authors. Holloway *et al.* (1985) measured nitrogen near the North West Shelf. They showed that the nitrogen concentration at the outer shelf and slope region was high below 100 m, but nitrogen concentration was low on the shelf. Rochford (1988) conducted further research in the same region and he showed that there were three types of waters; coastal water, subtropical water and tropical water. Among these, only tropical water was nitrate rich and this water was found in the slope region and near the bottom of the shelf region in summer. Tranter and Leech (1987) showed the results of the measurements of in vivo chlorophyll fluorescence (IVF), nutrients, oxygen, salinity and temperature on the North West Shelf (TL in Fig. 1). They showed that oxygen was rich but nitrate was very poor in the surface mixed layer and IVF had a maximum below the surface mixed layer which was about 100 m near the shelf edge and became shallower inshore in summer. Nutrients were not supplied from the coastal water but from the water at the shelf break.

Recently, Davis *et al.* (1991) estimated the survival rate of the larvae of southern bluefin tuna and diffusivity in a single patch by tracking it and sampling it repeatedly with the aid of a satellite tracked surface drifter (DA in Fig. 1). With all of these studies, however, we still do not have a clear understanding of how the juveniles of southern bluefin tuna are transported from the spawning ground to the nursery ground. Specifically, there appears to be no stable current which would carry larvae from the spawning ground to the nursery ground. It also is realized that information regarding to the feeding environment at the spawning ground is rather sparse. To understand how the stock of southern bluefin tuna is maintained, we started a multi-disciplinary study in 1992 and we present some of the results we obtained from the survey in 1992 in this paper.

2. Observation and Analysis

Observations were made from December, 1992 to February, 1993 using the research ship Shoyo-maru of the Japan Fishery Agency. The entire cruise was separated into three legs, from Japan to Darwin, Australia, from Darwin to Fremantle, Australia, and from Fremantle to Japan, for logistical reasons and for the accommodation of other surveys conducted during this cruise. The purposes of the observations of our group were to study the feeding environment at and around the spawning ground of southern bluefin tuna by CTD observations and chlorophyll measurements, and to study the mechanism which transports larvae of southern bluefin tuna from the spawning ground to the nursery ground by satellite tracked drifting buoys, the latter of which includes an estimation of dispersion in this region, which has never been done before. Figure 2 shows the locations of CTD stations, chlorophyll stations and the

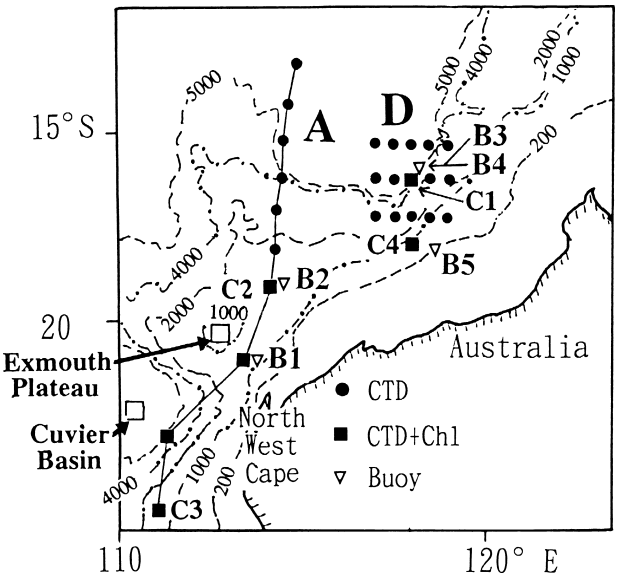

Fig. 2. Location of observations. Bathymetry in the region with contours at 200, 1000, 2000, 4000 and 5000 m is shown in this figure.

initial positions of drifting buoys (initial positions of B3 and B4 are the same). Area D in Fig. 2 is believed to be a center (not a geographical center) of a spawning ground of southern bluefin tuna, and this area was surveyed once during the first leg and once during the third leg of this cruise to study the feeding environment. The locations of CTD stations in the area D, shown as solid dots and a solid square, were the same in both legs. During each of these surveys, intensive biological observations, such as net samplings, were also conducted, but these are not discussed further in this paper. Line A was chosen to study the boundary between the area north of the Australian continent and the central Indian Ocean. As an initial survey to observe current field at the area D, one drifting buoy (B3) was released at the center of area D during the first leg. Four more drifting buoys were released during the third leg of the cruise. One of these buoys (B4) was released at the center of area D where B3 was released earlier. The positions of the release of B1 and B2 were chosen to study the current field in the area which was considered to be a down stream region of the spawning ground. The position of the release of B5 was chosen to study the current field further inshore than the spawning ground.

The drifting buoy had a window shade drogue which was 5 m long and 2 m wide and was connected to a surface float via the rope which was about 15 m long. A weight (50–60 kg) was attached to this drogue. The locations of these drifting buoys were measured by the Argos satellite system. The sampling interval was not uniform, but 67 to 76% of sampling intervals were less than 6 hours and 92 to 99% of sampling intervals were less than 12 hours. In the following analysis, data were interpolated with a one hour interval using Akima's spline method (IMSL) and then filters were applied to remove high frequency components unless otherwise mentioned.

To evaluate the effect of dispersion on the larval transport other than to estimate mean current fields from the trajectories of satellite tracked buoys, dispersion coefficients were evaluated by applying Lagrangian statistical techniques to the trajectories of satellite tracked buoys after computing auto-covariance. These methods have been discussed by many authors (Davis, 1983; Middleton, 1985; Krauss and Boning, 1987; Poulain and Niiler, 1989) and the following formulae were used here.

The u and v component in this paper refer to zonal and meridional current component, respectively. The Lagrangian integral time scale for u component is defined as

$$T_u = \int_0^{T_0} R(\tau)d\tau. \tag{1}$$

Here $R(\tau)$ is defined as

$$R(\tau) = \int_0^{T_m} u'(t)u'(t+\tau)dt \Big/ \left(\overline{u'^2}T_m\right) \tag{2}$$

where T_m is the length of the observation, T_0 the time at the first zero crossing of $R(\tau)$ and u' is the perturbation velocity, respectively. The overbar indicates a time average. From (1) and (2), the Lagrangian length scale for u component is defined as

$$L_u = \sqrt{\overline{u'^2}}\,T_L \tag{3}$$

and the Lagrangian zonal diffusivity is

$$K_{uu}(t) = \overline{u'^2}\int_0^t R(\tau)d\tau. \tag{4}$$

The Lagrangian statistical parameters of v component are defined similarly.

3. Results

Figure 3 shows the vertical distributions of temperature, salinity, oxygen and chlorophyll at three locations, shown as C1–3 in Fig. 2, as examples. Except for Fig. 3(a), these data were obtained during the same leg of the cruise. The surface temperature is about 28°C, the surface salinity is about 35.0 p.s.u. and the thickness of the surface mixed layer is about 20 to 40 m at the locations approximately north of 19°S (Fig. 3(a)). The stratification near the surface is mostly determined by temperature because salinity below the surface mixed layer is almost the same as salinity in the surface mixed

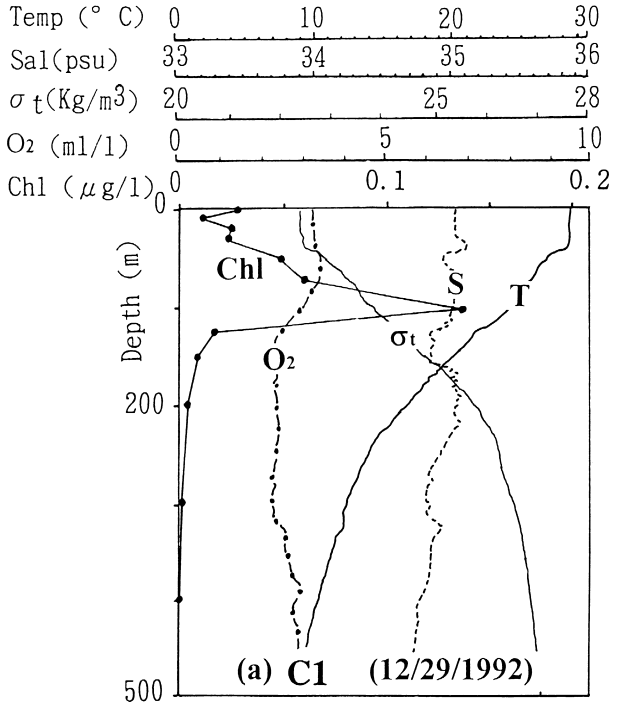

(a)

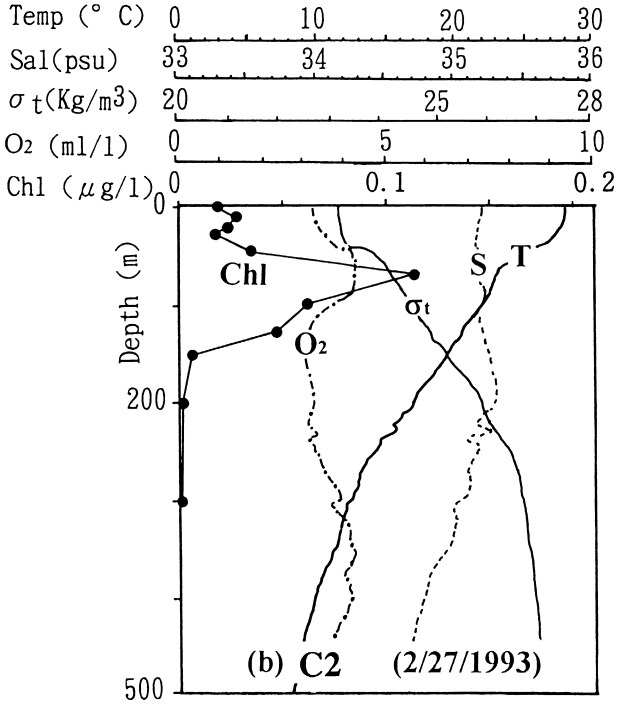

(b)

Fig. 3. The vertical distributions of temperature, salinity, σ_t, O_2 and chlorophyll at three locations; (a) C1, (b) C2 and (c) C3.

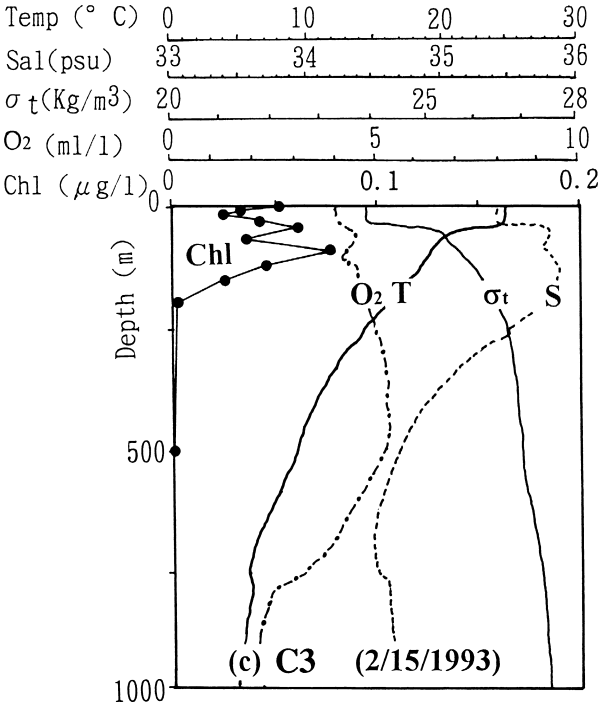

(c)

Fig. 3. (continued).

layer. There is a strong thermocline below the surface mixed layer to a depth of about 300 to 400 m. Salinity in the thermocline is relatively uniform, except for some small-scale perturbations of the thickness of about 10 to 20 m. At locations approximately south of 19°S (Fig. 3(c)), surface temperature is about 24°C and surface salinity is about 35.4 to 35.6 p.s.u. These values show that surface water at these southern stations has a lower temperature but a higher salinity than the surface water at northern stations. The thickness of surface mixed layer is about 20 to 50 m and salinity changes rapidly below the mixed layer at these southern stations. The maximum value of salinity is about 35.8 p.s.u. and the depth of the salinity maximum is in the thermocline. Salinity decreases gradually below its maximum. T-S diagrams show that both temperature and salinity differ considerably between northern and southern stations near the surface, but they converge at about 500 m.

The vertical distribution of chlorophyll concentration at all the stations show that chlorophyll concentration in the surface mixed layer is very poor but starts increasing beneath the bottom of the mixed layer, reaching a maximum at about 75–100 m. Below this maximum, chlorophyll decreases rapidly as depth increases and it becomes less than the value in the surface mixed layer at about 150 m. The thickness of the layer where chlorophyll content is larger than that in the mixed layer is about 100 m, except at one station (C4), where

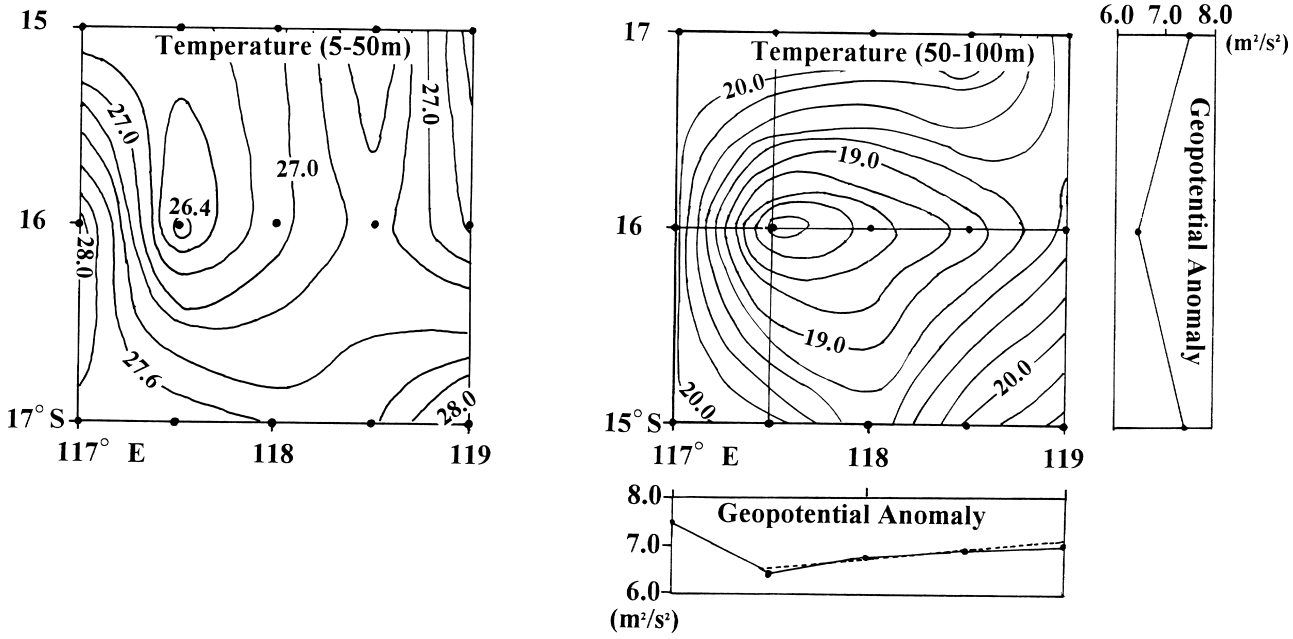

(a) (b)

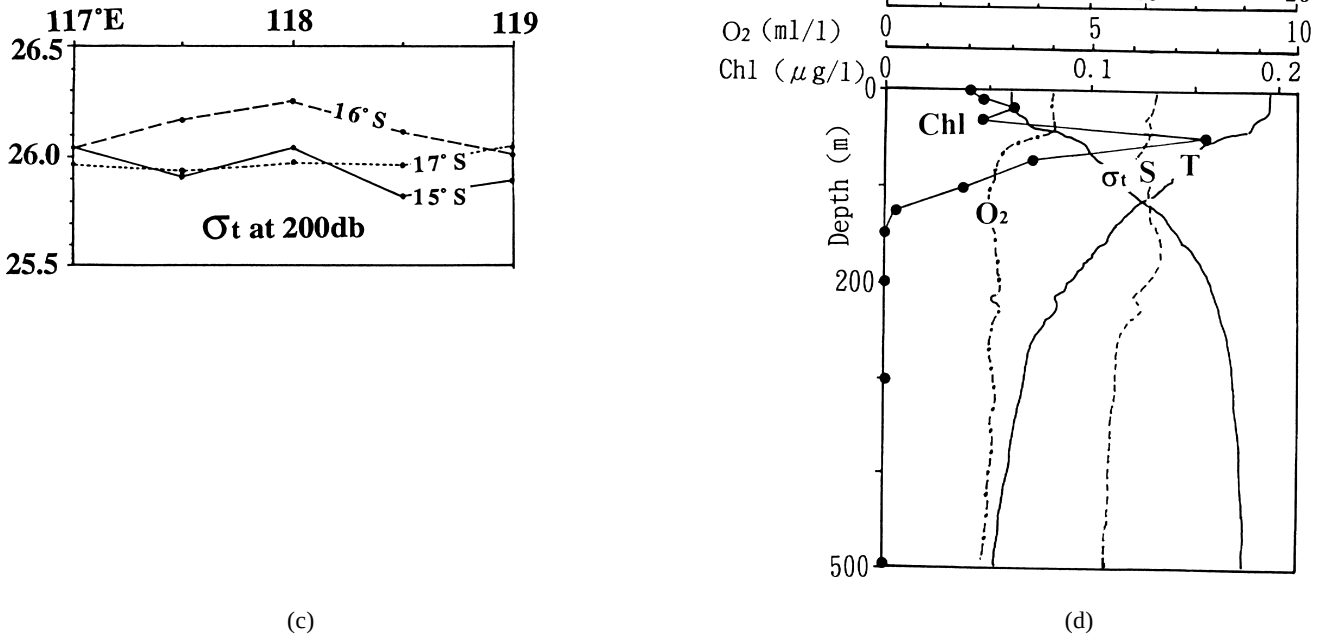

(c) (d)

Fig. 4. Horizontal distribution of temperature averaged over 5–50 m (a) and 50–100 m (b). Right and bottom panel of (b) are surface geopotential anomalies relative to 200 dB along solid lines shown in left panel. Zonal distribution of σ_t at 200 dB (c). Vertical distributions of temperature, salinity, σ_t, O_2 and chlorophyll at the central station (d). Solid dots indicate positions of observations.

the thickness is about 180 m. The maximum value appears to decrease at southern stations. The vertical distribution of oxygen shows a local maximum slightly below the bottom of the surface mixed layer at all the stations. Below this maximum, oxygen decreases at northern stations but increases at southern stations.

Figure 4 shows the horizontal distributions of temperature averaged vertically from 5 to 50 m (Fig. 4(a)) and 50 to 100 m (Fig. 4(b)) at the area D (Fig. 2). The buoy B4, the trajectory of which indicates that it was trapped in an eddy, was released during this leg of the cruise at the center of this figure (solid square, Fig. 2) where the CTD cast for Fig. 4(d) was conducted. The right and the bottom panel of Fig. 4(b) show the distribution of geopotential anomaly at the surface relative to 200 dB, which was the maximum depth of observations at all the stations except the central one (Fig. 4(d)), along the vertical and horizontal solid lines shown in the left panel, respectively. Figure 4(c) shows the zonal distribution of σ_t at 200 dB at 17°S, 16°S and at 15°S. Figure 4(d) shows the vertical distribution of temperature, salinity, oxygen and chlorophyll at C1 when this eddy was observed. The position where these data were taken is at the same position where data shown in Fig. 3(a) were taken.

Figure 5 shows the depth of isopycnal surfaces along line A (Fig. 2). This figure shows that surface density decreases towards the equator. Note that the depth of isopycnal surface of 27.0 decreases towards the equator. Figure 6 shows the surface geopotential anomalies along line A. The solid line in Fig. 6 is the result relative to 200 db and the dashed line is the result relative to 1000 db. To make comparison easier, a constant value, 9 m^2/s^2, is subtracted from the latter result. Figure 6 shows that the gradient of surface geopotential relative to 200 dB is almost the same as the gradient relative to 1000 dB which is equivalent to stating that the dynamic height at 200 dB is almost parallel to the dynamic height at 1000 dB. Along this line A, dynamic height increases towards the equator. The location of the local maximum appearing on this figure matches the location of a warm core eddy detected by a satellite image. As shown later, B1 was trapped in this eddy and stayed there until it stopped functioning (52 days).

Figure 7 shows the tracks of all the buoys released during this cruise. None of the buoys was transported to the south along the west coast of Australia. However, it is noted here that the juveniles of southern bluefin tuna were caught near the west coast of Australia at latitudes as far south as 33°S. The buoy B3 was released at the end of 1992 and ceased functioning by the end of February, 1993, which was about the time when other buoys were released. The buoys B1 and B4 were trapped in a counter-clockwise and a

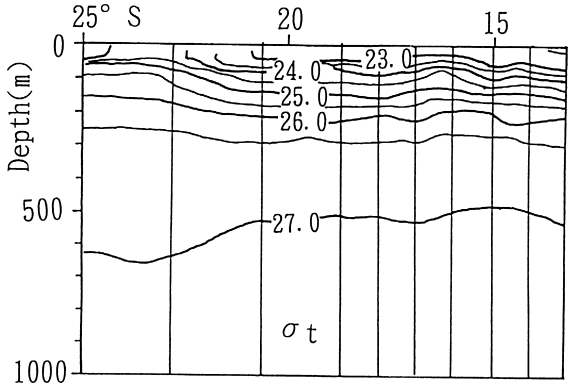

Fig. 5. The distribution of σ_t along the observation line A. The solid vertical lines show the positions of the observations.

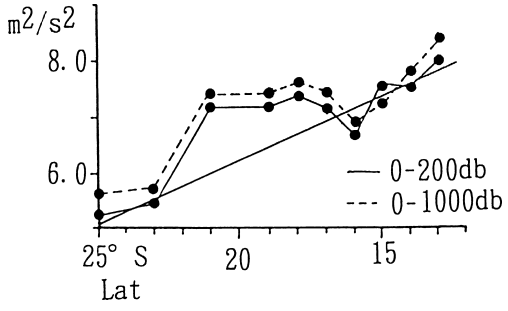

Fig. 6. Geopotential at the surface along line A relative to 200 dB (solid line) and relative to 1000 dB (dash line). A constant, 9 m^2/s^2 is subtracted from the results relative to 1000 db to make comparison easier. Solid straight line shows least square approximation computed by the values (0–200 dB) at 4 points north of 16°S and 2 points south of 23°S.

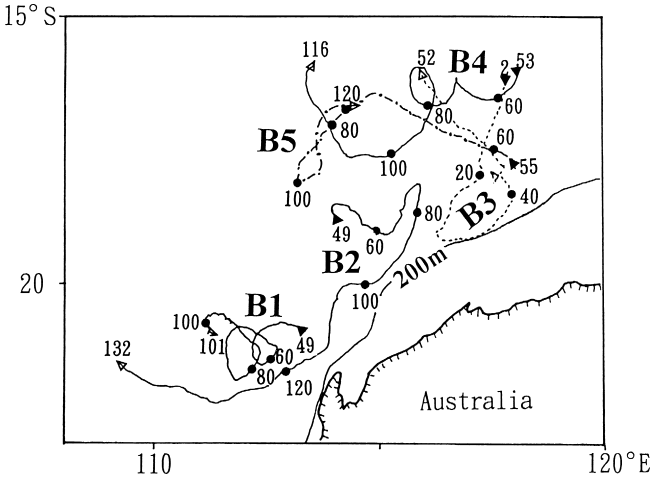

Fig. 7. Trajectories of surface drifting buoys. Solid circles are marked on each 20th day of Julian date. Numbers in the figure show each 20th day of Julian date, start dates and end dates. Solid triangles indicate initial positions and blank triangles indicate final positions.

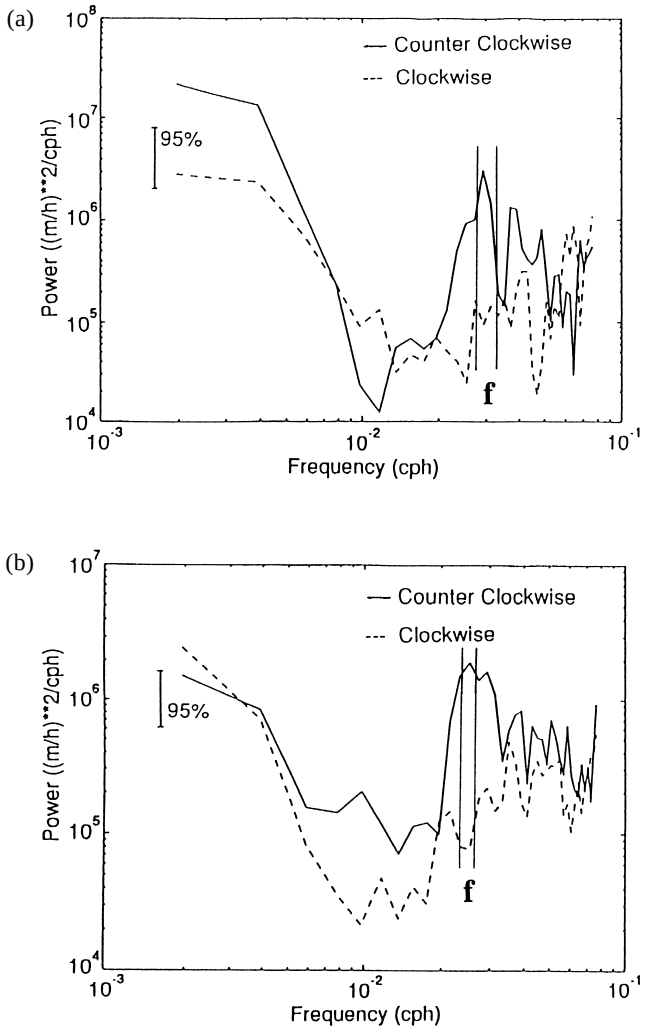

Fig. 8. Rotary spectra of velocities observed by (a) B1 and (b) B5. The solid line shows counter clockwise component and the dash line shows clockwise component. 95% confidence limit is shown in figure. The vertical lines labeled f indicate range of inertial frequency.

clockwise eddy, respectively. The periods of rotation of these eddies are approximately 20 days. The eddy which trapped buoy B1 was located along the line A as described above and moved westward very slowly. Figure 8 shows the rotary spectra of Lagrangian velocities obtained from B1 and B5. Peaks at inertial frequencies are rather broad (shown as **f** in the figure), but this is probably caused by the fact that inertial periods at these latitudes are very sensitive to the small changes of latitude (38.8 hours at 18°S and 43.5 hours at 16°S) rather than by the effect caused by the estimation of spectrum from Lagrangian measurement (Middleton, 1985). As described above, buoy B1 was trapped in the eddy and the counter-clockwise component is energetic near the lowest limit of frequencies in this figure.

Table 1. Lagrangian statistics obtained from trajectories of satellite tracked buoys.

Buoy	Start Julian days	End Julian days	Av-u cm/s	Av-v cm/s	Std-u cm/s	Std-v cm/s	T-u hours	T-v hours	L-u km	L-v km	K_{uu} 1×10^3 m^2/s	K_{vv} 1×10^3 m^2/s
B1	49	101	−4.82	1.97	18.8	18.2	62.4	65.2	27.8	26.9	3.44	3.07
B2	49	132	−4.91	−4.76	24.5	18.0	249.1	73.3	112.1	26.7	14.0	2.69
B3	2	52	−1.03	−5.57	22.3	19.5	66.8	96.7	33.0	46.2	4.54	6.14
B4	53	116	−8.56	0.312	16.4	17.9	83.0	93.6	33.1	44.8	3.67	5.97
B5	55	120	−7.05	0.244	21.3	15.9	274.4	162.7	126.4	58.7	1.62	5.88
Average	—	—	—	—	8.26	8.45	65.3	65.1	29.2	28.7	3.66	3.53

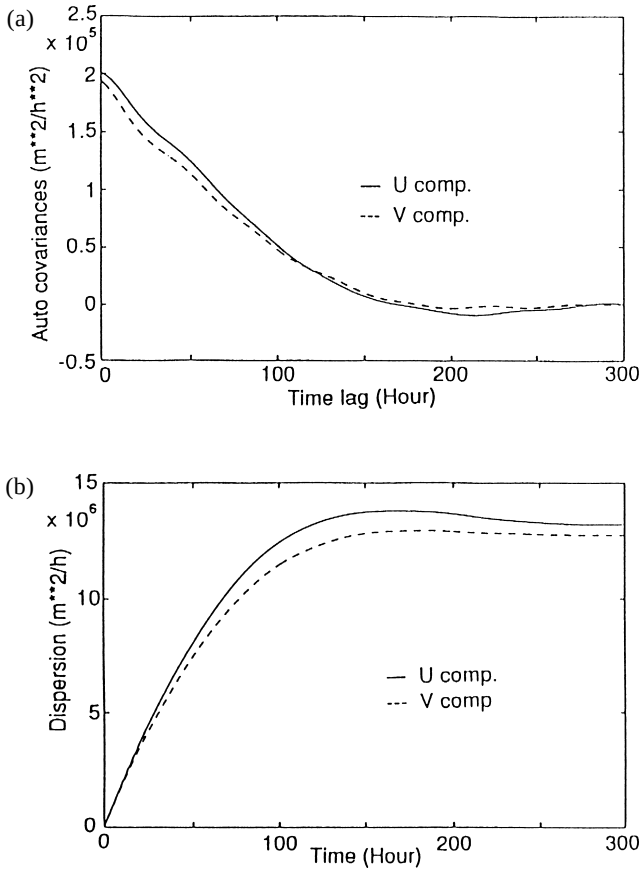

Fig. 9. (a) Averaged Lagrangian auto-covariances of *u* component (solid line) and *v* component (dash line) as a function of time lag. (b) Averaged Lagrangian dispersion (diffusivity) computed from the results of (a).

Table 1 shows some statistical values computed from these data after a 35-hour running mean was applied. Mean drifting velocities in the zonal direction, shown as Av-u in Table 1, are westward, while mean drifting velocities in the meridional direction, Av-v in Table 1, are either northward or southward and four buoys out of five have larger mean zonal than meridional speeds. The standard deviations of the velocities have relatively small differences between meridional (shown as Std-u in Table 1) and zonal components (Std-v). The Lagrangian integral time scales, shown as T-u and T-v in Table 1, of buoys B2 and B5 are several times larger than the others. This is caused by the fact that T_0 of these buoys are larger than the others. The Lagrangian length scales (shown as L-u and L-v in Table 1) of B2 and B5 are also large because of these large Lagrangian time scales. Auto-correlation functions $R(\tau)$ of these buoys decrease rapidly initially, as those of the other buoys do, but they then oscillate slightly above zero. These result in somewhat larger values of Lagrangian diffusivities, shown as K_{uu} and K_{vv} in Table 1. For further analyses, records of individual buoys are divided into record segments of length 300 hours to increase the degree of freedom (Poulain and Niiler, 1989). From these records, the averaged covariance is calculated, as shown in Fig. 9(a). In these computations, a 5-pole Butterworth filter with cutoff frequency at 45 hours was applied to remove inertial oscillation. The results of these computations are shown at the bottom row (shown as Average in Table 1) of Table 1. Figure 9(b) shows dispersion coefficients computed from these auto-covariances. This figure shows that dispersion coefficients initially increase almost linearly and then they become almost flat after about 150 hours. The differences between zonal and meridional components are relatively small.

4. Discussion

4.1 Oceanographic condition near the spawning ground

The surface water in the northern portion of this year's observation area appears to have its origin in tropical water. The satellite images taken during the cruise show that relatively warm water spread in the entire area between Australia and Indonesia. The southern limit of this warm water shifted slightly northward to the west of the North West Cape. The satellite images also show that warm water extended southward along the west coast from the North West Cape. Relatively low salinity water below 100 m at locations approximately north of 19°S seems to originate from the tropical east Indian Ocean (Rochford, 1988). The characteristic of this water is low in salinity and oxygen but high in nitrate. Past research has shown that the surface tropical water is nutrient poor (Tranter and Leech, 1987; Rochford, 1988) and the maximum of chlorophyll is below the mixed layer because of the availability of nutrient. Our results indicate that the chlorophyll distribution in the spawning ground of southern bluefin tuna is similar to that observed further inshore on shelf and near the shelf break.

Figure 4(d) shows that the temperature in the eddy below the mixing layer is 3–5°C lower than the time when there is no eddy (Fig. 3(a)). Figures 3(a), 4(a), 4(b) and 4(d) suggest that the temperature contrast of this eddy in the surface layer is not as prominent as in the thermocline. This is probably due to strong heating at the surface due to the tropical climate. This relatively obscure thermal signature at the surface may make it difficult to detect this eddy by SST alone. Figure 4(d) also shows that chlorophyll concentration in the eddy is larger than the time when there is no eddy (Fig. 3(a)). One of the possible causes is the supply of nutrients from a lower layer due to the eddy. Geostrophic computation from this geopotential anomaly at the eastern four points using a least square linear approximation (dashed line in the bottom panel of Fig. 4(b)), indicates that the geostrophic current at the surface relative to 200 dB is 8.7 cm/s. Counting the effects of the movement of the eddy (westward at about 10 cm/s estimated from the position on Julian date 60

and 80) and the time duration between observations (about 20 hours), it changes from 8.7 to 10.0 cm/s. The trajectory of B4 suggests that surface velocity due to the circular motion is about 17 cm/s. The difference between these two values can be either due to the barotropic motion or the choice of the reference level. The horizontal distribution of σ_t at 200 dB (Fig. 4(c)) shows the signature of this eddy, although it is much smaller than at shallower depths, and this suggests that the motion of this eddy reaches more than 200 dB.

The near stationary eddy which trapped B1 was located very close to Exmouth Plateau, which has a peak at 20°S and 113°E, and Cuvier Basin, which is located south west of Exmouth Plateau (Fig. 2). From the map, it appears that this eddy was not located above the plateau but above Cuvier Basin, which has a roughly circular shape. A similar, near stationary counter-clockwise eddy has been reported earlier (Metso *et al*., 1986; Quadfasel *et al*., 1996) and these eddies may be caused by these local topographic features. This topographic system may have an influence on the transport of larvae of southern bluefin tuna in this region through the effects on a flow field.

The characteristic of surface geopotential field along line A shown in Figure 6 is qualitatively in agreement with previous research (Thompson, 1984; Godfrey and Ridgway, 1985). The gradient of steric sea level east of the North West Cape computed by Godfrey and Ridgway (1985) is relatively weak. This tendency matches the description that warm tropical water spreads from the Timor sea to the Indian Ocean. Geostrophic computation using linear approximation with a least square method applied to the data along line A, excluding those in the eddy (shown as a solid straight line in Fig. 6), shows that the surface current is approximately 4 cm/s eastward relative to 200 dB. This eastward geostrophic flow across the line A matches the results of both Thompson (1984) and Godfrey and Ridgway (1985). However, the trajectory of B1 indicates a weak westward mean flow and the trajectory of B2 indicates a relatively strong westward flow across the line A (Fig. 7). The contradiction between the track of B1 and the geostrophic current may be explained by the westward migration of an isolated eddy which is fairly commonly observed (Joyce, 1991) although it can migrate eastward, too (Nof, 1983; Killworth, 1986). Using Nof's solution, estimated migration speed of the eddy which trapped B1 is westward at 1.9 cm/s if the radius of this eddy is 1 degree latitude and is westward at 2.4 cm/s if the radius of this eddy is 2 degrees latitude. Here, the internal Rossby radius of deformation of the first baroclinic mode is 41 km which is numerically evaluated by solving the vertical mode equation (e.g. Gill, 1982). There still exists a discrepancy between the current obtained from the track of B1 and geostrophic current after subtracting this migration speed. This discrepancy may result from the selection of reference level for the geostrophic computation. Considering the slope of σ_t = 27.0, we may have to take a reference level deeper than 1000 dB. It also is possible that some of the assumptions required for Nof's solution may not be appropriate for this eddy. The contradiction between the track of B2 and the geostrophic current may result from the temporal variation of the current field or from the selection of reference level for the geostrophic computation. It is noted that similar tracks of drifting buoys were observed by CSIRO in the past.

4.2 Larval transport

It appears that the meso-scale energy of the surface current field in the spawning ground of southern bluefin tuna is dominant, while the mean flow is weak. Our computation shows that dispersion coefficients reach 3500–3600 m^2/s. These values are comparable to those off California (Poulain and Niller, 1989). This feature can be seen on maps of trajectories of drifters in previous research (Vaudrey *et al*., 1983; Metso *et al*., 1986; Quadfasel *et al*., 1996; Michida and Yoritaka, 1996). Figures 32 and 33 in Nishikawa *et al*. (1985) show that the distribution of larvae of southern bluefin tuna south of 13.5°S does not change much, while the distribution of larvae at the latitude around 10°S extends westward, which is probably due to the SEC. Our present results show that mean flow near the spawning ground of southern bluefin tuna is westward during the observation period. By this mean flow alone, the majority of larvae are probably carried towards the central Indian Ocean from the spawning ground, rather than towards the Australian coast. One of the possible mechanisms which maintain the stock is that larvae are dispersed by strong local meso-scale current fields and some of them arrive close to the shore before they are carried away to the central Indian Ocean. Once larvae are carried near the North West Cape but close enough to the coast, the Leeuwin current (Boland *et al*., 1988; Smith *et al*., 1991) may carry them along the west coast of Australia toward the nursery ground. Smith *et al*. (1991) showed the existence of the Leeuwin current at the shelf break off the North West Cape (SB, Fig. 1).

It is noted that almost none of buoys described in the publications cited above moved from the spawning ground of southern bluefin tuna to the nursery ground. Figure 6 in Quadfasel *et al*. (1996) shows that buoys located within a very narrow range from the coast at 115°E moved towards the southwest and only one of them eventually moved southward along the west coast of Australia. Therefore, larvae must be very close to the coast when they arrive off the North West Cape for the mechanism described above to work. Figure 36 in Nishikawa *et al*. (1985) shows a large concentration of larvae at 113.5°E, 18.5°S, at 115.5°E, 10.5°S and at 119.5°E, 16.5°S. The first position is slightly west of North West Cape, and the second position is off Java, where upwelling events are common. The third position is about 590 km north east of North West Cape. The larvae at

the first and the second position are quite likely being carried towards the central Indian Ocean by SEC. Therefore the question is whether the larvae at the third position can be dispersed and reach close to the coast when they arrive off the North West Cape. After substituting the observed dispersion coefficient and mean speed into a simple advection/diffusion analytical model (Appendix), we estimated that about 0.8% of larvae or drifting buoys released at the third position can reach within 10 km from the coast off the North West Cape, where the shelf width is about 5 km. It is noted here that with the advection speed obtained from the tracks of our drifting buoys, it takes about 120 days to arrive off North West Cape from this third position, and 120 days is much longer than the length of the juvenile stage of a southern bluefin tuna (20 days, Davis *et al*., 1991). Therefore, the above estimate may be useful to interpret the tracks of drifting buoys but caution must be taken in interpreting the above estimate for the transport of larvae of southern bluefin tuna.

After superimposing a bathymetry map onto a trajectory map of drifting buoys (e.g. Quadfasel *et al.*, 1996), it appears that the 200 m isobath almost limits shoreward excursion of buoys. This, and the T-S distributions across the shelf shown by several authors (e.g. figures in Fieux *et al*., 1996) suggests the existence of a current along the shelf break north east of North West Cape. However, the direction of this current and its variation are not clear from previous research. Figure 4 in Quadfasel *et al*. (1996) and Figure 3 of Fieux *et al*. (1996) both indicate several current reversals near the shelf break. Further studies are necessary to evaluate the effects of current along the shelf break on the larval transport of southern bluefin tuna.

5. Conclusion

The surface at the spawning ground of southern bluefin tuna was covered by warm tropical water. The thickness of the surface mixed layer was about 20–50 m and the chlorophyll concentration in this layer was low. The maximum chlorophyll concentration was found at 75–100 m. The maximum of oxygen was found at depths slightly below the bottom of the surface mixed layer. The eddy observed in the spawning ground had a radius of over 160 km (1.5 degree latitude) and reached over 200 dB. The chlorophyll content in the eddy was highest among all the observations we had conducted. The temperature contrast of this eddy at the surface was not as prominent as at depths below the surface mixed layer. The trajectories of satellite tracked buoys showed that meso-scale variability was dominant with weak westward mean flow. The dispersion coefficient which was estimated from these trajectories increased linearly at first but reached a maximum, 3.6×10^3 m^2/s, at 150 hours. The Lagrangian time scale was about 65 hours and the Lagrangian length scale was about 29 km.

Our results indicate that mean flow at the spawning ground is westward and with this mean flow alone, larvae are more probably carried towards the central Indian Ocean rather than the nursery ground. However, meso-scale current variations are dominant at the spawning ground and this may suggest that the observed dispersion due to the meso-scale current variations could be an important mechanism in maintaining the stock of southern bluefin tuna. Further studies of currents in the Timor sea are necessary to evaluate environmental effects on the recruitment of southern bluefin tuna. It is possible that past research, including ours, may have missed currents near the coast. It also is noted that our evaluation of dispersion coefficients is made on the basis of very limited data. It is necessary to re-evaluate, using more data. Recent studies indicate that there are significant inter-annual variabilities in this region. It is quite possible that these inter-annual variabilities have significant effects on the recruitment of the fish stock through the changes of water properties, mean current fields and meso-scale current fields which is dominant at the spawning ground of southern bluefin tuna.

Acknowledgements

We would like to express our appreciation to the help given by Drs. Furushima, Kimura, Kishi and Nakata at Ocean Research Institute, University of Tokyo, and the captain and crew of JFA research ship Shoyo-maru for their efforts in the conduct of our surveys under the heavy sea. Some of the computations were done on computers at Engan Kaiyou Chousa Kabushikigaisha (Coastal Ocean Research Co.) and we thank them for their courtesy. We would also like to express our appreciation to an editor and anonymous reviewers who provided useful comments and information as well as their constructive criticism in refining this paper.

Appendix

To evaluate the effects of the dispersion, let us assume that current (advection) is uniform in time and space and ignore the dispersion along the coast. From the result of drifting buoys, the averaged current field is roughly parallel to the Australian coast. Therefore, we approximate the region as an infinitely long band with two boundaries at the north and south in which the Australian coast is a southern boundary at $y = 0$ and the Indonesian coast is a northern boundary at $y = M$. The x axis is along the Australian coast, positive towards the central Indian Ocean (roughly westward). The equation of dispersion is then

$$\frac{\partial C}{\partial t} + u\frac{\partial C}{\partial x} = \frac{\partial}{\partial y}\left(K\frac{\partial C}{\partial y}\right) - \alpha C \qquad \text{(A1)}$$

where C is the concentration, u the advection speed, t the time, K the horizontal eddy dispersion coefficient normal to the coast and α is the mortality. The dispersion coefficient, K, is a function of time and space and

$$K = \kappa t y \qquad \text{for } 0 \le y < L \text{ and } 0 \le t < t_0$$

$$K = \kappa t L \qquad \text{for } L \le y \le M \text{ and } 0 \le t < t_0$$

$$K = \kappa t_0 y \qquad \text{for } 0 \le y < L \text{ and } t_0 \le t$$

$$K = \kappa t_0 L = \text{constant} \qquad \text{for } L \le y \le M \text{ and } t_0 \le t \qquad \text{(A2)}$$

where κ is a constant, L the distance from the coast where the effect of the coast vanishes and M is the width of the domain, 1700 km. This form of K reproduces the linear increase of dispersion coefficient in time during the initial period, as observed, and the linear increase of the component of dispersion coefficient normal to the coast near the coast (Davis, 1985). L is 100 km, which is a size of eddies observed and the scale of shelf width. t_0 is 150 hours, from observation (Table 1). The value of κ was chosen so that $\kappa t_0 L$ matches the value estimated from observation, 3.6×10^3 m^2/s (Table 1). The no flux condition ($K\partial C/\partial y = 0$) is applied at both boundaries. As matching conditions, both C and $K\partial C/\partial y$ are continuous at $y = L$.

The solution of (A1) for the observer moving with an advection speed, whose position is $x = ut$, is

$$C = \mathrm{e}^{\left(-\int_0^t \alpha d\tau\right)}\left[\kappa\int_0^t \tau P d\tau + \sum_{n=1}^{\infty}\left\{\frac{\kappa}{Jo\left(2\sqrt{\lambda_n L}\right)}\int_0^t \tau P \mathrm{e}^{\kappa\lambda_n\left(\tau^2-t^2\right)/2} d\tau\phi_n\right\}\right]$$

for $0 \le y < L$ and $0 \le t < t_0$

$$C = \mathrm{e}^{\left(-\int_0^t \alpha d\tau\right)}\left[-\frac{\kappa L}{M-L}\int_0^t \tau P d\tau + \frac{1}{M-L}\int_L^M Co dy + \sum_{n=1}^{\infty}\left\{\left[-\frac{2\kappa L}{M-L}\int_0^t \tau P \mathrm{e}^{\kappa L\gamma_n\left(\tau^2-t^2\right)/2} d\tau + \frac{2}{M-L}\mathrm{e}^{-\kappa L\gamma_n t^2/2}\int_L^M Co\Phi_n dy\right]\Phi_n\right\}\right]$$

for $L \le y \le M$ and $0 \le t < t_0$

$$C = \mathrm{e}^{\left(-\int_0^t \alpha d\tau\right)}\left[\kappa\int_{t_0}^t P d\tau + a_0 + \sum_{n=1}^{\infty}\left\{\left[\frac{\kappa}{Jo\left(2\sqrt{\lambda_n L}\right)}\int_{t_0}^t P \mathrm{e}^{\kappa\lambda_n(\tau-t)} d\tau + a_n \mathrm{e}^{-\kappa\lambda_n\left(t-t_0\right)}\right]\phi_n\right\}\right]$$

for $0 \le y < L$ and $t_0 \le t$

$$C = \mathrm{e}^{\left(-\int_0^t \alpha d\tau\right)}\left[-\frac{\kappa L}{M-L}\int_{t_0}^t P d\tau + b_0 + \sum_{n=1}^{\infty}\left\{\left[-\frac{2\kappa L}{M-L}\int_{t_0}^t P \mathrm{e}^{\kappa L\gamma_n(\tau-t)} d\tau + b_n \mathrm{e}^{-\kappa L\gamma_n\left(t-t_0\right)}\right]\Phi_n\right\}\right]$$

for $L \le y \le M$ and $t_0 \le t$ (A3)

where

$\phi_n = Jo\,(2\sqrt{\lambda_n y})$,
$\Phi_n = \cos\{\sqrt{\gamma_n}\,(y - L)\}$,
$\gamma_n = (n\pi/(M-L))^2$,
$a_0 = \kappa\int_0^{t_0} \tau P d\tau$,

$$a_n = \frac{\kappa}{Jo\left(2\sqrt{\lambda_n L}\right)}\int_0^{t_0} \tau P e^{\kappa\lambda_n\left(\tau^2-t_0^2\right)/2} d\tau$$

$$b_0 = -\frac{\kappa L}{M-L}\int_0^{t_0} \tau P d\tau + \frac{1}{M-L}\int_L^M Co dy,$$

$$b_n = -\frac{2\kappa L}{M-L}\int_0^{t_0} \tau P e^{\kappa L\gamma_n\left(\tau^2-t_0^2\right)/2} d\tau + \frac{2}{M-L} e^{-\kappa L\gamma_n t_0^2/2}\int_L^M Co\Phi_n dy,$$

λ_n, an eigenvalue which satisfies $J_1(2\sqrt{\lambda_n L}) = 0$, *Jo* the Bessel function of order of 0 and J_1 is the Bessel function of order of 1. The mortality, α, is assumed to be a function of time alone (or a constant). *Co* is the initial distribution of *C* and is assumed to be zero for $0 \le y < L$. We used gaussian distribution of a unit volume with a half amplitude width of 2W as an initial distribution, C_0. In this case,

$$\int_L^M Co\Phi_k dy = e^{-\frac{1}{4r}\gamma_k}\cos\left(\sqrt{\gamma_k}(Yo-L)\right)$$

where $r = -(1/W^2)\ln(1/2)$ and *Yo* is the position of the center of the distribution, respectively.

From the matching condition, a function *P*, which is proportional to the flux at $y = L$, satisfies

$$\kappa\sum_{n=1}^{\infty}\left\{\int_0^t \tau P e^{\kappa\lambda_n(\tau^2-t^2)/2}d\tau\right\}+\frac{2\kappa L}{M-L}\sum_{n=1}^{\infty}\left\{\int_0^t\left[\tau P e^{\kappa L\gamma_n(\tau^2-t^2)/2}\right]d\tau\right\}+\frac{\kappa M}{M-L}\int_0^t\tau P d\tau$$
$$=\frac{1}{M-L}\int_L^M Co\,dy+\frac{2}{M-L}\sum_{n=1}^{\infty}\left\{e^{-\kappa L\gamma_n t^2/2}\int_L^M Co\Phi_n dy\right\}$$

for $0 \le t < t_0$

$$\kappa\sum_{n=1}^{\infty}\left\{\int_{t_0}^t\left[P e^{\kappa\lambda_n(\tau-t)}\right]d\tau\right\}+\frac{2\kappa L}{M-L}\sum_{n=1}^{\infty}\left\{\int_{t_0}^t\left[P e^{\kappa L\gamma_n(\tau-t)}\right]d\tau\right\}+\frac{\kappa M}{M-L}\int_{t_0}^t P d\tau$$
$$=\left\{b_0+\sum_{n=1}^{\infty}\left(b_n e^{-\kappa L\gamma_n(t-t_0)}\right)\right\}-\left\{a_0+\sum_{n=1}^{\infty}\left(\frac{a_n}{Jo\left(2\sqrt{\lambda_n L}\right)}e^{-\kappa\lambda_n(t-t_0)}\right)\right\}$$

for $t_0 \le t$. (A4)

This solution was obtained by the method of eigenfunction expansion. Further descriptions of derivation as well as the methods of computation may be published in a separate paper elsewhere.

Let us assume larvae (drifting buoys) are trapped within a short distance, *l*, from the coast off the North West Cape will be transported to the nursery ground through Leeuwin current. The shelf width off North West Cape is very narrow (~5 km) and close to the internal Rossby radius of deformation on the North West Shelf which is estimated to be about 10 km from the data shown in Tranter and Leech (1986) and Cresswell *et al*. (1993) and it is a typical scale of various coastal phenomena (e.g. Gill, 1982). Therefore, let us chose *l* to be 10 km. Further, let us assume that the center of initial distribution is located 400 km from the coast and the width of the half amplitude point of the initial distribution is 100 km for the standard case.

Figure A1 shows the time series of *C* integrated from $y = 0$ to $y = 10$ km for the dispersion coefficient evaluated from Table 1 ($\kappa_0 L = 3.6 \times 10^3$ m^2/s; (i), solid curve), for the case when the dispersion coefficient is 10 times larger ((ii), solid line with solid circles), for the case when the dispersion is half of the standard case ((iii), dash line), and for the case when the width of the half amplitude point is 200 km with the standard value of dispersion coefficient ((iv), fine line), respectively. For comparison, the result for the case when

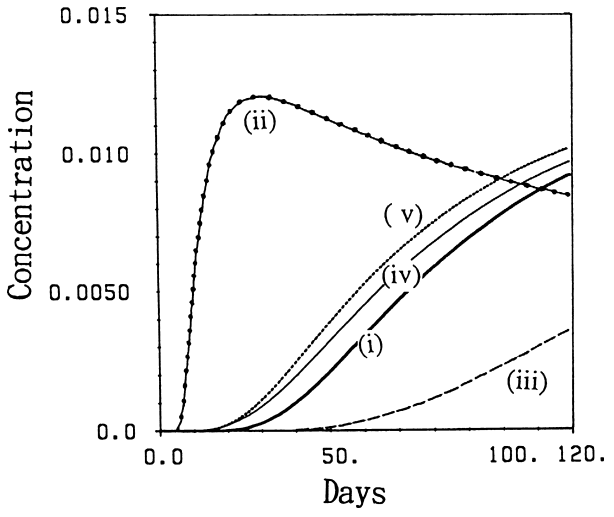

Fig. A1. (a): Concentration integrated from 10 km offshore to the coast as a function of time for an observer moving with an advection speed for the standard case ((i); solid curve), for the case when dispersion coefficient is 10 time larger ((ii); solid line with solid circles), for the case when dispersion is half of the standard case ((iii), dash line), and for the case when the width of the half amplitude point is 200 km with the standard value of dispersion coefficient ((iv); fine line), respectively. For the case when dispersion coefficient is constant is shown as dot line (v).

the dispersion coefficient is constant in space and time is also shown in this figure as a dotted line (v). Mortality, α, is set to 0 for all of the cases. The final value, when the concentration becomes uniform is about 0.0058, and all the cases shown here overshoot this value.

References

Andrews, J. C. (1977): Eddy structure and the West Australian Current. *Deep-Sea Res*., **24**, 1133–1148.

Boland, F. M., J. A. Church, A. M. G. Forbes, J. S. Godfrey, A. Huyer, R. L. Smith and N. J. White (1988): Current-meter data from the Leeuwin Current interdisciplinary experiment. *CSIRO Mar. Lab. Rep*., **198**.

Cresswell, G. R. and T. J. Golding (1980): Observations of a south-flowing current in the southeastern Indian Ocean. *Deep-Sea Res*., **27A**, 449–466.

Cresswell, G. R., A. Frische, J. Peterson and D. Quadfasel (1993): Circulation in the Timor Sea. *J. Geophys. Res*., **98**, 14379–14389.

Davis, R. E. (1983): Oceanic property transport, Lagrangian particle statistics, and their prediction. *J. Mar. Res*., **41**, 163–194.

Davis, R. E. (1985): Drifter observations of coastal surface currents during code: The statistical and dynamical views. *J. Geophys. Res*., **90**, 4756–4772.

Davis, T. L. O., V. Lyne and G. P. Jenkins (1991): Advection, dispersion and mortality of a patch of southern bluefin tuna larvae *Thunnus maccoyii* in the East Indian Ocean. *Mar. Ecol. Prog. Ser*., **73**, 33–45.

Fieux, M., R. Molcard and A. G. Ilahude (1996): Geostrophic transport of the Pacific-Indian Oceans throughflow. *J. Geophys. Res*., **101**, 12421–12432.

Gill, A. E. (1982): *Atmosphere—Ocean Dynamics*. Academic Press, London, 662 pp.

Godfrey, J. S. (1996): The effect of the Indonesian throughflow on ocean circulation and heat exchange with the atmosphere: A review. *J. Geophys. Res*., **101**, 12217–12237.

Godfrey, J. S. and K. R. Ridgway (1985): The large-scale environment of the poleward-flowing Leeuwin Current, western Australia: Longshore steric height gradients, wind stresses and geostrophic flow. *J. Phys. Oceanogr*., **15**, 481–495.

Godfrey, J. S. and A. J. Weaver (1991): Is the Leeuwin Current driven by Pacific heating and winds? *Prog. Oceanogr*., **27**, 225–272.

Hamon, B. V. (1965): Geostrophic currents in the south-eastern Indian Ocean. *Aust. J. Mar. Freshwater Res*., **16**, 255–271.

Hautala, S. L., J. L. Reid and N. Bray (1996): The distribution and mixing of Pacific water masses in the Indonesian Seas. *J. Geophys. Res*., **101**, 12375–12389.

Holloway, P. E. and H. C. Nye (1985): Leeuwin Current and wind distributions of the southern part of the Australian North West Shelf between January 1982 and July 1983. *Aust. J. Mar. Freshwater Res*., **36**, 123–137.

Holloway, P. E., S. E. Humphries, M. Atkinson and J. Imberger (1985): Mechanisms for nitrogen supply to the Australian North West Shelf. *Aust. J. Mar. Freshwater Res*., **36**, 753–764.

Joyce, T. M. (1991): Review of U.S. contributions to warm-core rings. *Rev. Geophys*., **Supplement**, 610–616.

Killworth, P. D. (1986): On the propagation of isolated multilayer and continuously stratified eddies. *J. Phys. Oceanogr*., **16**, 709–716.

Krauss, W. and C. W. BÒning (1987): Lagrangian properties of eddy fields in the northern North Atlantic as deduced from satellite-tracked buoys. *J. Mar. Res*., **45**, 259–291.

Lukas, R., T. Yamagata and J. P. McCreary (1996): Pacific low-latitude western boundary currents and the Indonesian throughflow. *J. Geophys. Res*., **101**, 12209–12216.

McCreary, J. P., S. R. Shetye and P. K. Kundu (1986): Thermohaline forcing of eastern boundary currents: With application to the circulation off the west coast of Australia. *J. Mar. Res*., **44**, 71–92.

Metso, A., G. S. Wells, D. J. Vaudrey and G. R. Cresswell (1986): Satellite-tracked buoy data, July 1982 to September 1984. *CSIRO Mar. Lab. Rep*., **180**, 50 pp.

Meyers, G. (1996): Variation of Indonesian throughflow and the El-Niño—Southern oscillation. *J. Geophys. Res*., **101**, 12255–12263.

Michida, Y. and H. Yoritaka (1996): Surface currents in the area of the Indo-Pacific throughflow and in the tropical Indian Ocean observed with surface drifters. *J. Geophys. Res*., **101**, 12475–12482.

Middleton, J. F. (1985): Drifter spectra and diffusivities. *J. Mar. Res*., **43**, 37–55.

Nishikawa,Y., M. Honma, S. Ueyanagi and S. Kikawa (1985): Average distribution of larvae of oceanic species of scombrid fishes, 1956–1981. *Far Seas Fish. Res. Lab S. Ser*., **12**.

Nof, D. (1983): On the migration of isolated eddies with application to Gulf Stream rings. *J. Mar. Res*., **41**, 399–425.

Poulain, P. M. and P. P. Niller (1989): Statistical analysis of the surface circulation in the California Current system using satellite-tracked drifters. *J. Phys. Oceanogr*., **19**, 1588–1603.

Quadfasel, D., A. Frische and G. Cresswell (1996): The circulation in the source area of the South Equatorial Current in the eastern Indian Ocean. *J. Geophys. Res*., **101**, 12483–12488.

Rochford, D. J. (1988): Seasonal influx of nitrates to the slope and shelf waters off North-West Australia. CSIRO Mar. Lab. Rep., **191**.

Shinguu, C. (1981): Ecology and stock of southern bluefin tuna. *CSIRO Mar. Lab. Rep*., **131**.

Smith, R. L., A. Huyer, J. S. Godfrey and J. A. Church (1991): The Leeuwin Current off Western Australia, 1986–1987. *J. Phys. Oceanogr*., **21**, 323–345.

Tchernia, P. (1980): *Descriptive Regional Oceanography*. Pergamon Press, 253 pp.

Thompson, R. O. R. Y. (1984): Observations of the Leeuwin Current off Western Australia. *J. Phys. Oceanogr*., **14**, 623–628.

Tranter, D. J. and G. S. Leech (1987): Factors influencing the standing crop of phytoplankton on the Australian Northwest Shelf seaward of the 40 m isobath. *Contin. Shelf Res*., **7**, 115–133.

Vaudrey, D. J., G. S. Wells and G. R. Cresswell (1983): Satellite-tracked buoy data report IX South-West Pacific and Indian Oceans and Great Australian Bight January to June 1982. *CSIRO Mar. Lab. Rep*., **159**, 19 pp.

Wyrtki, K. (1961): Scientific Results of Marine Investigations of the South China Sea and the Gulf of Thailand. NAGA Report 2.